Applied Mathematical Modelling 76 (2019) 479–494

Contents lists available at ScienceDirect

Applied Mathematical Modelling

journal homepage: www.elsevier.com/locate/apm

Design of a coordinated adaptive backstepping tracking control for nonlinear uncertain active suspension system

Hui Pang*, Xu Zhang, Jianan Chen, Kai Liu

School of Mechanical and Precision Instrument Engineering, Xi'an University of Technology, Xi'an 710048, China

ARTICLE INFO

Article history:
Received 19 December 2018
Revised 14 June 2019
Accepted 17 June 2019
Available online 22 June 2019

Keywords:
Vehicle active suspension
Adaptive backstepping control
Tracking control
Stability analysis

ABSTRACT

This paper presents a novel adaptive backstepping tracking control for nonlinear uncertain active suspension system, which can achieve the coordinated control over the sprung-mass acceleration and suspension dynamic displacement for nonlinear uncertain active suspension system based on a developing model-reference system. First, according to adaptive backstepping control principle, this model-reference system is designed with purpose of providing the ideal reference trajectories for the sprung-mass displacement and vertical velocity, respectively. Then, the design of a coordinated adaptive backstepping tracking controller is conducted to make the control plant accurately track the prescribed performances of the model-reference system by virtue of the backstepping technique and Lyapunov stability theory, in which a virtual controller with online parameter regulation rules is designed and implemented to guarantee the stability of vehicle body. Finally, a numerical example is provided to verify the effectiveness of our designed adaptive backstepping tracking controller under various operating scenarios.

1. Introduction

It is well known that vehicle suspension system plays an essential role in guaranteeing vehicle maneuverability and stability, as well as providing better ride quality and absorbing vibration energies generated by the external road excitation [1–3]. Compared with passive and semi-active suspension, active suspensions can not only produce active control force via actuators to inhibit vibration caused by uneven road surfaces, but also increase suspension travel to change the chassis layout and then deteriorate the suspension performance. Although active suspensions are usually regarded as an effective way to improve vehicle dynamics performance and have been intensively investigated in [4–6], it is still a challenging issue in developing the control strategies for vehicle active suspension system.

During the past years, a number of various control approaches applied in active suspension systems have been a hot research topic. For instance, the authors in [7] designed an H_∞ optimal controller to improve riding comfort and handling stability, and the effectiveness and feasibility are verified by the experimental results. In [8], the authors designed a full-car active suspension controller with a reduced order observer by combing sliding-mode control and fuzzy logic control. Based on the nonlinear backstepping technique, another control approach in [9] was proposed to achieve a better trade-off between the ride comfort and safety constraints on suspension system. Considering different road profile inputs, the authors in [10] proposed a new road-adaptive nonlinear control for a half-car active suspension system by employing the road-adaptive algorithms.

* Corresponding author.
E-mail address: panghui@xaut.edu.cn (H. Pang).

https://doi.org/10.1016/j.apm.2019.06.030
0307-904X/

In the aforementioned literatures, vehicle suspension system is usually simplified as a linear dynamics model. However, for active suspension system, on the one hand, it is actually a typical nonlinear system subjected to various road surface disturbances [11–13]. Specifically, suspension springs and dampers possess obvious nonlinear features when running on different road surfaces at different speeds, which may cause some difficulties in modeling of vehicle suspension system. Additionally, the sprung-mass may change with the changeable passenger numbers or dynamic loads, thus it is essentially the parameter uncertainties of vehicle suspension system, which increases the modeling errors, and then results in inaccuracies of the controller design and further leads to the instability of active suspension control system [14–16]. Therefore, it is an interesting and challenging study in developing the appropriate adaptive backstepping controller for active suspension system.

On the other hand, the adaptive backstepping technique has been extensively utilized in the controller design for nonlinear uncertain systems because of such merits like anti-input saturation, interference suppression, accurate control, good robustness over the conventional control approaches [17–21]. Particularly, it has higher reliability in dealing with ongoing variations in the tracking control of the grade-connection nonlinear system with the external disturbances. In [22], the control problem of quarter-vehicle semi-active suspension system was investigated using backstepping technique, and an adaptive output-feedback controller was developed by combining the designed observer and state-feedback controller, meanwhile, the theoretical results were confirmed by several simulation tests. The authors in [23] presented an adaptive backstepping control design for active suspension systems with the unknown body mass and coefficients of tire dynamics to deal with the nonlinearity of the hydraulic actuator. In a similar way, to solve the input nonlinearity of the hydraulic active suspension system, a master-slave control law consisting of a robust H_∞ controller and an adaptive backstepping controller was proposed through a nonlinear separation strategy, wherein the former was referred to the master controller and the latter one was referred to the slave controller, and the effectiveness of the proposed approach was illustrated by a realistic design example [24].

To sum up, although there are some literatures reporting the adaptive backstepping control for active suspension system, yet less attention has been paid on the adaptive backstepping controller with considering the suspension's safety performance constraints. Note that this may impose great effects on the stability of active suspension system if the control force exceeds its maximum limit [25]. It is worth mentioning that, an adaptive backstepping control strategy in [26] was proposed for vehicle active suspension with hard constraints, wherein the multi-objective control of vehicle semi-active suspension was conducted by planning a specific reference trajectory. However, this controller design is not aimed at controlling the unsprung mass. Additionally, our group has proposed a new adaptive backstepping-based tracking controller using Quadratic-Lyapunov function for a half-vehicle model considering the nonlinearity characteristics of suspension system [27]. As demonstrated in [27], the proposed adaptive backstepping-based tracking controller (ABC) has better ride quality and safety constraint, as well as tracking performances. Yet, there are also some disadvantages like being higher conservatism, and only being suitable for the fixed initial values of the closed-loop control system. Specifically, it is hard to achieve coordinated control over sprung-mass acceleration and suspension dynamic displacement, simultaneously. For this reason, it is interesting to develop a novel adaptive backstepping tracking controller to improve vehicle handling stability.

However, there are few studies on how to manage the tradeoffs between vehicle ride comfort and handling stability with regarding to the effects of uncertain parameters on the controlled suspension system. To this end, a novel adaptive backstepping tracking control design is proposed for nonlinear uncertain vehicle active suspension with aiming to coordinately control over the sprung-mass acceleration and suspension dynamic displacement, simultaneously. Based on the established nonlinear active suspension dynamics model, a model-reference system (MRS) is developed to provide an ideal reference trajectory. Further, a virtual controller with online parameter regulation rules is designed to achieve the accurate tracking of the preset performance of the MRS, and it is then taken as the input of the proposed adaptive backstepping tracking controller based on *proj.* operator. The main contributions of this paper lie in the following two aspects:

(1) An MRS is constructed to provide the ideal reference trajectories by introducing a high-pass and low-pass filter.
(2) A new adaptive backstepping tracking control is design to achieve the coordinated control over the sprung-mass acceleration and suspension dynamic displacement, meanwhile, the proposed controller can well make the control plant accurately track the prescribed performances of the MRS and then to eliminate the negative effects of the model uncertainties on the closed-loop control system.

The remainder of this paper is organized as follows: Section 2 presents system modeling and problem formulation. Section 3 addresses the adaptive backstepping controller synthesis in detail. The simulation investigation and discussion are performed in Section 4. Lastly, Section 5 contains the conclusions and suggestions for future work.

2. System modeling and problem formulation

2.1. Nonlinear quarter-vehicle active suspension model

The nonlinear quarter-vehicle model is depicted in Fig. 1, which has been extensively used in various studies because of its simplicity and ability to capture many essential characteristics of a real suspension system.

In Fig. 1, $M_s(t)$ and m_u are the sprung and unsprung mass. $z_s(t)$, $z_u(t)$ and $z_r(t)$ are the displacement of sprung mass, unsprung mass and the road input disturbance, respectively. $F_s(z_s,z_u,t)$ is the elastic force produced by the nonlinear spring

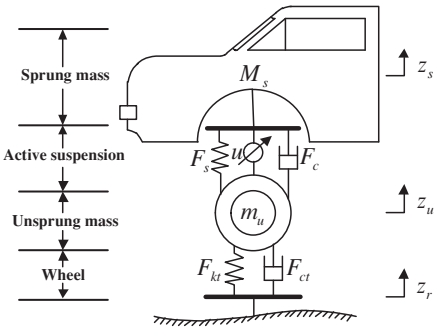

Fig. 1. The dynamics model of quarter-vehicle active suspension.

among the suspension components, $F_c(\dot{z}_s, \dot{z}_u, t)$ is the damping force produced by the piece-wise linear function that models the general MR damper, $u(t)$ denotes the active control input, $F_{kt}(z_u,z_r,t)$ and $F_{ct}(\dot{z}_u, \dot{z}_r, t)$ are the tire elastic force and damping force, respectively.

Based on Newton's second law, the dynamics equations of this control plant is given by

$$\begin{cases} M_s(t)\ddot{z}_s = -F_s(z_s, z_u, t) - F_c(\dot{z}_s, \dot{z}_u, t) + u(t), \\ m_u\ddot{z}_u = F_s(z_s, z_u, t) + F_c(\dot{z}_s, \dot{z}_u, t) - F_{kt}(z_u, z_r, t) - F_{ct}(\dot{z}_u, \dot{z}_r, t) - u(t) \end{cases} \tag{1}$$

wherein the mathematical expression of $F_s(z_s,z_u,t)$ and $F_c(\dot{z}_s, \dot{z}_u, t)$, $F_{kt}(z_u,z_r,t)$ and $F_{ct}(\dot{z}_u, \dot{z}_r, t)$ are respectively defined as follows [16,27]:

$$F_s(z_s, z_u, t) = k_s(z_s(t) - z_u(t)) + k_{ns}(z_s(t) - z_u(t))^3 \tag{2}$$

$$F_c(\dot{z}_s, \dot{z}_u, t) = \begin{cases} c_{s1}(\dot{z}_s(t) - \dot{z}_u(t)), & (\dot{z}_s(t) - \dot{z}_u(t)) > 0 \\ c_{s2}(\dot{z}_s(t) - \dot{z}_u(t)), & (\dot{z}_s(t) - \dot{z}_u(t)) \le 0 \end{cases} \tag{3}$$

$$F_{kt}(z_u, z_r, t) = k_t(z_u(t) - z_r(t)) \tag{4}$$

$$F_{ct}(\dot{z}_u, \dot{z}_r, t) = c_t(\dot{z}_u(t) - \dot{z}_r(t)) \tag{5}$$

where k_s is the linear spring rigidity coefficient, k_{ns} is the spatial stiffness coefficient, c_{s1} and c_{s2} stand for the damping coefficients when extending and compressing the piecewise linear damper, respectively, k_t and c_t are the tire stiffness coefficient and the damping coefficient, respectively.

Define the state variables as $x_1(t)=z_s(t)$, $x_2(t)=\dot{z}_s(t)$, $x_3(t)=z_u(t)$ and $x_4(t)=\dot{z}_u(t)$. Then, from (1), the state-space equation of quarter-vehicle suspension is expressed by

$$\begin{cases} \dot{x}_1(t) = x_2(t) \\ \dot{x}_2(t) = \dfrac{1}{M_s(t)}(-F_s(z_s, z_u, t) - F_c(\dot{z}_s, \dot{z}_u, t) + u(t)) \\ \dot{x}_3(t) = x_4(t) \\ \dot{x}_4(t) = \dfrac{1}{m_u}(F_s(z_s, z_u, t) + F_c(\dot{z}_s, \dot{z}_u, t) - F_{kt}(z_u, z_r, t) - F_{ct}(\dot{z}_u, \dot{z}_r, t) - u(t)) \end{cases} \tag{6}$$

Due to the variations of passenger numbers and vehicle body loads, $M_s(t)$ is always changed, thus it is determined as the uncertain parameters of the control plant in this article, and it is assumed that the lower and upper bounds of $M_s(t)$, denoted as M_{smin} and M_{smax}, satisfy

$$M_s(t) \in \{M_s(t) : M_{s\min} \le M_s(t) \le M_{s\max}\} \tag{7}$$

2.2. Problem formulation

For this active suspension system, the control objectives can be summarized as follows:

(1) With aiming to manage the tradeoffs between ride comfort and handling stability of the active suspension system, an MRS is designed to provide the ideal reference trajectories of the sprung-mass displacement and vertical velocity.
(2) The designed controller should be robust and adaptable to the nonlinearities of suspension system and the uncertainties of sprung mass, as well as the different road surfaces.
(3) To ensure the safety performance constraints of this active suspension system, the following three conditions should be satisfied. That is, the dynamic tire load should not exceed the static loads as

$$|F_{kt}(z_u, z_r, t) + F_{ct}(\dot{z}_u, \dot{z}_r, t)| < F_{\text{static}} \tag{8}$$

where the static loads $F_{\text{static}}= (M_s(t)+m_u)g$.

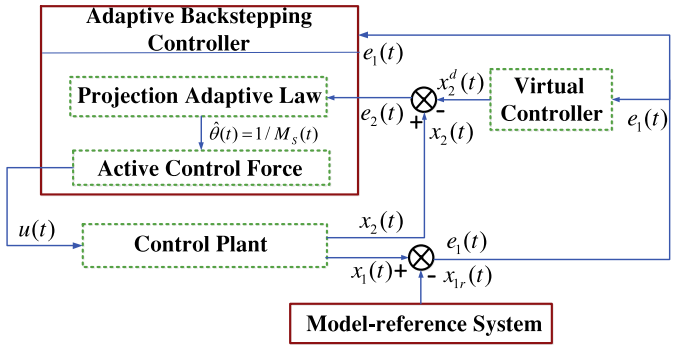

Fig. 2. Control scheme of the proposed CABT controller.

Next, due to the limit of suspension mechanical structure, the suspension dynamic displacement should be less than the allowable suspension travel, i.e.

$$|z_s(t) - z_u(t)| \le \Delta y_{\max} \tag{9}$$

where $\Delta y_{\max}$ represents the maximum value of the suspension dynamic displacement.

Furthermore, the actuator control force should not exceed its maximal value, which is expressed by

$$|u(t)| \le u_{\max} \tag{10}$$

3. The controller synthesis

3.1. The block diagram of the control system

The block diagram of the proposed coordinated adaptive backstepping tracking (CABT) controller is shown in Fig. 2. Note that this CABT controller includes the subsystems such as the control plant, the MRS and the adaptive backstepping controller and virtual controller.

3.2. The MRS design

To begin with, we need to design an MRS to achieve the tradeoff between the ride comfort and handling stability and then make these two performance indexes vary with the road disturbances adaptively. To distinguish the state vectors of the control plant from the counterpart of the MRS, $x_{1r}(t)$, $x_{2r}(t)$, $x_{3r}(t)$, and $x_{4r}(t)$ are used to replace with $x_1(t)$, $x_2(t)$, $x_3(t)$, and $x_4(t)$, respectively, thus the first control objective J_1 in the MRS can be described as

$$J_1 = W_1(s)x_{1r}(t) + W_2(s)(x_{1r}(t) - x_{3r}(t)) \tag{11}$$

where $W_1(s)$ is the high-pass filter and $W_2(s)$ is the low-pass filter, and the design ideas of $W_1(s)$ and $W_2(s)$ are derived from literature [16,20,28], and thus they can be determined as

$$W_1(s) = \frac{s}{s + \varepsilon_{10} + c_1 f_1(x_{1r}(t) - x_{3r}(t))} \tag{12}$$

$$W_2(s) = \frac{\varepsilon_{20} + c_2 f_2(x_{1r}(t) - x_{3r}(t))}{s + \varepsilon_{20} + c_2 f_2(x_{1r}(t) - x_{3r}(t))} \tag{13}$$

Note that c_1 and c_2 are positive constant. Based on the control requirement of sprung-mass acceleration, the smaller values $\varepsilon_{10}+c_1\, f_1(x_{1r}(t)-x_{3r}(t))$ and $\varepsilon_{20}+c_2\, f_2(x_{1r}(t)-x_{3r}(t))$ are first selected, and then they can be regulated in terms of suspension dynamic displacement. When the suspension dynamic displacement gets larger, the values of $\varepsilon_{10}+c_1\, f_1(x_{1r}(t)-x_{3r}(t))$ and $\varepsilon_{20}+c_2\, f_2(x_{1r}(t)-x_{3r}(t))$ will increase, thereby narrowing the frequency passband of $W_1(s)$ and enlarging the frequency passband of $W_2(s)$, and then the proportion of the suspension dynamic displacement in J_1 is increased, and furthermore the proportion of the sprung-mass displacement is reduced. On the contrary, when the suspension dynamic displacement becomes smaller, this will result in the decreasing of $\varepsilon_{10}+c_1\, f_1(x_{1r}(t)-x_{3r}(t))$ and $\varepsilon_{20}+c_2\, f_2(x_{1r}(t)-x_{3r}(t))$ along with the reduction in the proportion of the suspension dynamic displacement, and the increasing in the proportion of the sprung-mass displacement.

Define the nonlinear function $f_1(x_{1r}(t)-x_{3r}(t))$ and $f_2(x_{1r}(t)-x_{3r}(t))$ in $W_1(s)$ and $W_2(s)$ as

$$f_1(x_{1r}(t) - x_{3r}(t)) = \begin{cases} \left(\frac{x_{1r}(t)-x_{3r}(t)-l_1}{l_2}\right)^3 & x_{1r}(t) - x_{3r}(t) > l_1 \\ 0 & |x_{1r}(t) - x_{3r}(t)| \le l_1 \\ -\left(\frac{x_{1r}(t)-x_{3r}(t)+l_1}{l_2}\right)^3 & x_{1r}(t) - x_{3r}(t) < -l_1 \end{cases} \tag{14}$$

$$f_2(x_{1r}(t)-x_{3r}(t))=\begin{cases}\left(\frac{x_{1r}(t)-x_{3r}(t)-n_1}{n_2}\right)^3 & x_{1r}(t)-x_{3r}(t)>n_1\\ 0 & |x_{1r}(t)-x_{3r}(t)|\le n_1\\ -\left(\frac{x_{1r}(t)-x_{3r}(t)+n_1}{n_2}\right)^3 & x_{1r}(t)-x_{3r}(t)<-n_1\end{cases} \tag{15}$$

where l_1, l_2, n_1 and n_2 are positive constants satisfying $l_1>n_1$.

Next, to improve the adaptiveness and robustness of the designed MRS, the backstepping adaptive control technique is adopted to minimize J_1.

Let

$$\begin{cases}y_1(t)=W_1(s)x_{1r}(t)\\ y_2(t)=W_2(s)(x_{1r}(t)-x_{3r}(t))\end{cases} \tag{16}$$

By taking derivative of Eq. (16), one gets

$$\begin{cases}\dot{y}_1(t)=x_{2r}(t)-\varepsilon_1 y_1(t)\\ \dot{y}_2(t)=\varepsilon_2(x_{1r}(t)-x_{3r}(t)-y_2(t))\end{cases} \tag{17}$$

where $\varepsilon_1=\varepsilon_{10}+c_1 f_1(x_{1r}(t)-x_{3r}(t))$ and $\varepsilon_{20}+c_2 f_2(x_{1r}(t)-x_{3r}(t))$, synthesizing (11), (16) and (17) gives

$$\dot{J}_1(t)=x_{2r}(t)-\varepsilon_1 y_1(t)+\varepsilon_2(x_{1r}(t)-x_{3r}(t)-y_2(t)) \tag{18}$$

Note that $x_{2r}^d(t)$ is taken as the virtual control input in (20), and $x_{2r}^d(t)$ is defined as

$$x_{2r}^d(t)=-d_1 J_1+\varepsilon_1 y_1(t)-\varepsilon_2(x_{1r}(t)-x_{3r}(t)-y_2(t)) \tag{19}$$

where d_1 is a positive constant.

Generally, there exists an error between $x_{2r}(t)$ and $x_{2r}^d(t)$ in the MRS. Thus, define the second control objective $J_2(t)$ as

$$J_2(t)=x_{2r}(t)-x_{2r}^d(t) \tag{20}$$

Substituting (18) into (20) gives

$$\dot{J}_1(t)=-d_1 J_1(t)+J_2(t) \tag{21}$$

Derivating along (20) and using (6) result in

$$\dot{J}_2(t)=-\frac{1}{M_s(t)}(F_s(z_s,z_u,t)+F_c(\dot{z}_s,\dot{z}_u,t)-u_m(t))-\dot{x}_{2r}^d(t) \tag{22}$$

The control input function $u_m(t)$ in the MRS is designed as

$$u_m(t)=-M_s(t)d_2 J_2(t)-M_s(t)J_1(t)+F_s(z_s,z_u,t)+F_c(\dot{z}_s,\dot{z}_u,t)+M_s(t)\dot{x}_{2r}^d(t) \tag{23}$$

where d_2 is a positive constant.

Substituting (23) into (22) yields

$$\dot{J}_2(t)=-d_2 J_2(t)-J_1(t) \tag{24}$$

The control objectives consisting of (21) and (24) in the MRS are as follows:

$$\begin{cases}\dot{J}_1(t)=-d_1 J_1(t)+J_2(t)\\ \dot{J}_2(t)=-d_2 J_2(t)-J_1(t)\end{cases} \tag{25}$$

Define a positive Lyapunov function as

$$V_{\mathrm{MRS}}(J_1,J_2)=\frac{1}{2}J_1^2(t)+\frac{1}{2}J_2^2(t) \tag{26}$$

Differentiating (26) and substituting (21) and (24) into (26), one can obtain

$$\dot{V}_{\mathrm{MRS}}(J_1,J_2)=-d_1 J_1^2(t)-d_2 J_2^2(t)<0 \tag{27}$$

Since $V_{\mathrm{MRS}}(J_1J_2)$ is positive definite while $\dot{V}_{\mathrm{MRS}}(J_1,J_2)$ is negative definite, thus $J_1(t)$ and $J_2(t)$ will reach the global asymptotic stability, i.e., when $t\to\infty$, $J_1(t)\to 0$, $J_2(t)\to 0$.

3.3. The CABT controller design

Step 1: In this step, our goal is to determine the control input $u(t)$ and the adaptive control law $\dot{\hat{\theta}}(t)$ for the designed CABT controller.

First, define the tracking error $e_1(t)=x_1(t)$-$x_{1r}(t)$, if e_1 tends to be zero, which means that $x_1(t)$ can better track the reference trajectory $x_{1r}(t)$, for the vertical motion of the control plant, we have

$$\begin{cases}\dot{x}_1(t)=x_2(t)\\ \dot{x}_2(t)=\theta(t)(-F_s(z_s,z_u,t)-F_c(\dot{z}_s,\dot{z}_u,t)+u(t))\end{cases} \tag{28}$$

where the uncertain parameter $\theta(t)=\frac{1}{M_s(t)}\in[\theta_{\min}\ \theta_{\max}]$, $\theta_{\min}=\frac{1}{M_{s\max}}$ and $\theta_{\max}=\frac{1}{M_{s\min}}$.

After differentiating $e_1(t)$, we have

$$\dot{e}_1(t)=x_2(t)-\dot{x}_{1r}(t) \tag{29}$$

Similarly, define the reference trajectory $x_2^d(t)$ for the virtual control input $x_2(t)$ in (29), and the tracking error of vertical velocity is given by $e_2(t)=x_2(t)-x_{2r}^d(t)$, then we have

$$\dot{e}_1(t)=e_2(t)+x_2^d(t)-\dot{x}_{1r}(t) \tag{30}$$

Next, $x_2^d(t)$ is defined as

$$x_2^d(t)=\dot{x}_{1r}(t)-k_1\tanh(e_1(t)) \tag{31}$$

where k_1 is a positive constant.

Define the Lyapunov function as

$$V_1=\frac{1}{2}e_1^2(t) \tag{32}$$

Derivating along V_1 gives

$$\dot{V}_1(t)=e_1(t)e_2(t)-k_1e_1(t)\tanh(e_1(t)) \tag{33}$$

It is obvious that $\dot{V}_1=-k_1e_1(t)\tanh(e_1(t))\le 0$ with $e_2(t)$=0, and the tracking error $e_1(t)$ will approach zero asymptotically.

Therefore, we could get an appropriate $u(t)$ to make $x_2(t)$ to accurately track $x_2^d(t)$, even though there exists an uncertain parameter $\theta(t)$ in (28).

Derivating $e_2(t)$ and using (6) result in

$$\dot{e}_2(t)=\theta(t)(-F_s(z_s,z_u,t)-F_c(\dot{z}_s,\dot{z}_u,t)+u(t))-\ddot{x}_{1r}(t)+k_1(1-\tanh^2(e_1(t)))\dot{e}_1(t) \tag{34}$$

To achieve the control objectives, $u(t)$ is designed as

$$u(t)=\frac{1}{\hat{\theta}(t)}(\ddot{x}_{1r}(t)-k_1(1-\tanh^2(e_1(t)))\dot{e}_1(t)-k_2\tanh(e_2(t))-e_1(t))+F_s(z_s,z_u,t)+F_c(\dot{z}_s,\dot{z}_u,t) \tag{35}$$

where k_2 is a positive constant and $\hat{\theta}(t)$ is the estimation value of $\theta(t)$.

The adaptive control law based on the *proj*. operator is designed as [27]

$$\dot{\hat{\theta}}(t)=\text{Projection}_{\hat{\theta}(t)}(r\tau(t)) \tag{36}$$

where $r>0$ is the tuning parameter for the adaptive control law and $\tau(t)=(-F_c(z_s,z_u,t)-F_c(\dot{z}_s,\dot{z}_u,t)+u(t))e_2(t)$.

The *proj*. operator $\text{Projection}_{\hat{\theta}(t)}(r\tau(t))$ is given by

$$\text{Projection}_{\hat{\theta}(t)}(r\tau(t))=\begin{cases}0, & \text{if } \hat{\theta}(t)=\theta_{\max} \text{ and } r\tau(t)>0,\\ 0, & \text{if } \hat{\theta}(t)=\theta_{\min} \text{ and } r\tau(t)<0,\\ r\tau(t), & \text{other case}\end{cases} \tag{37}$$

Step 2: Conduct the stability analysis of the designed CABT controller to ensure that it can reach stability state within a finite time by using $u(t)$ and $\dot{\hat{\theta}}(t)$. To this end, define the Lyapunov function as

$$V_2=V_1+\frac{1}{2}e_2^2(t)+\frac{1}{2r}\tilde{\theta}^2(t) \tag{38}$$

where $\tilde{\theta}(t)=\hat{\theta}(t)-\theta(t)$.

By derivating V_2, we have

$$\dot{V}_2=\dot{V}_1+e_2(t)\dot{e}_2(t)+r^{-1}\tilde{\theta}(t)\dot{\hat{\theta}}(t)\le -k_1e_1(t)\tanh(e_1(t))-k_2e_2(t)\tanh(e_2(t))\le 0 \tag{39}$$

For (39), integrating the left and right side from zero to any time $t>0$ concurrently, results in

$$V_2=\int_0^t\dot{V}_2d\tau+V_2(0)\le V_2(0) \tag{40}$$

Table 1
The parameters of quarter-vehicle active suspension.

Symbol	Definition	Value
M_s	Sprung mass	360 kg
m_u	Unsprung mas	59 kg
k_s	Nonlinear spring stiffness coefficient	20,000 N · m^{-1}
k_{ns}	Nonlinear spring spatial stiffness coefficient	200,000 N·m^{-1}
k_t	Tire stiffness coefficient	190,000 N·m^{-1}
c_t	Tire damping coefficient	1000 Ns·m^{-1}
c_{s1}	Viscous damping when extending	1200 Ns·m^{-1}
c_{s2}	Viscous damping when compressing	800 Ns·m^{-1}

It can be observed that $e_1(0)$ and $e_2(0)$ are bounded, which is expressed by

$$|e_1(t)| \le \sqrt{2V_2(0)}, |e_2(t)| \le \sqrt{2V_2(0)} \tag{41}$$

From (41), we can get

$$\begin{cases} |x_1(t)| \le \|x_{1r}(t)\|_\infty + \sqrt{2V_2(0)} \\ |x_2(t)| \le \|\dot{x}_{1r}(t)\|_\infty + (k_1+1)\sqrt{2V_2(0)} \end{cases} \tag{42}$$

Afterwards, we have

$$-F_s(z_s, z_u, t) - F_c(\dot{z}_s, \dot{z}_u, t) + u(t) \in L_\infty \tag{43}$$

That is, $\dot{e}_2(t) \in L_\infty$. By further derivating (39), we get

$$\begin{aligned} \ddot{V}_2 \le & -k_1 e_1(t)(1-\tanh^2(e_1(t)))\dot{e}_1(t) - k_1\dot{e}_1(t)\tanh(e_1(t)) \\ & - k_2 e_2(t)(1-\tanh^2(e_2(t)))\dot{e}_2(t) - k_2\dot{e}_2(t)\tanh(e_2(t)) \end{aligned} \tag{44}$$

In terms of (44), we can arrive at the conclusion that $\dot{V}_2$ is uniformly continuous for $\ddot{V}_2 \in L_\infty$, and moreover, it is easily derived from Barbalat lemma and its postulation [29] that with $t \to \infty$, $\dot{V}_2 \to 0$. That is, the tracking errors of $e_1(t)$ and $e_2(t)$ will converge to asymptotic stability.

4. Simulation investigation and discussion

In this section, a numerical example is provided to demonstrate the effectiveness of the proposed CABT controller under different operating conditions. The model parameters are given in Table 1, the CABT controller parameters are selected as $r = 0.001$, $k_1 = k_2 = 10$, $\theta_{\min} = 1/420$ kg, and $\theta_{\max} = 1/330$ kg, and $\hat{\theta}(0) = 390$, $\Delta y_{\max} = 0.05$ m, $u_{\max} = 3000$ N. Moreover, the MRS parameters are determined as $l_1 = 0.05$, $l_2 = 0.03$, $n_1 = 0.005$, $n_2 = 0.02$, $d_1 = d_2 = 200$, $c_1 = 0.02$, $c_2 = 0.1$, $\varepsilon_{10} = 1$ Hz, and $\varepsilon_{20} = 2$ Hz.

To reveal the control effects of the proposed CABT controller in achieving the vehicle body stabilization and disturbance attenuation performance, the following comparative simulations for this quarter-vehicle model are performed under random and bump road disturbances, respectively. In the research field of vehicle dynamics and control, the road disturbance input is usually modeled as a random input signal, and a bump input signal [25], which are based on the criterion of ISO 9996:1996 [30].

(1) The comparative studies between the designed CABT controller, the common sliding model controller (SMC), and the passive suspension (PS) system under random, and bump road disturbances, respectively, which are sequentially presented in Sections 4.1 and 4.2.
(2) To further reveal the advantages of the proposed CABT controller against the classical ABC in [16], and the designed ABC in [27], the comparative simulations are carried out under the same random and bump road disturbances, respectively, which are presented in Section 4.3.

4.1. Performance of the CABT controller under random road

Herein, the mathematical formula of the random road disturbance is borrowed from [25] and given by

$$\dot{z}_r(t) = 2\pi n_0 \sqrt{G_q(n_0)V}\, w(t) \tag{45}$$

where $\pi = 3.14$; $n_0 = 0.1$(1/m) is the reference spatial frequency; $G_q(n_0)$ stands for the road roughness coefficient with a value of 256×10^{-6} m^3 for C-class road; $V = 20$ m/s is the vehicle forward speed. $w(t)$ is zero mean white Gaussian noise with identity power spectral density.

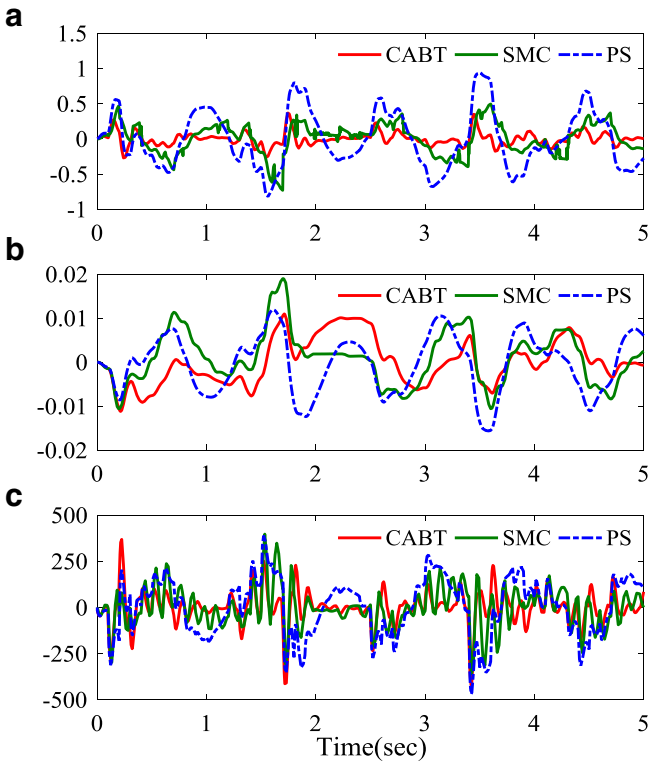

Fig. 3. The responses of (a) sprung-mass acceleration (m/s^2), (b) suspension dynamic displacement (m) and (c) tire dynamic load (N) for the CABT, SMC and PS system under C-class road disturbance.

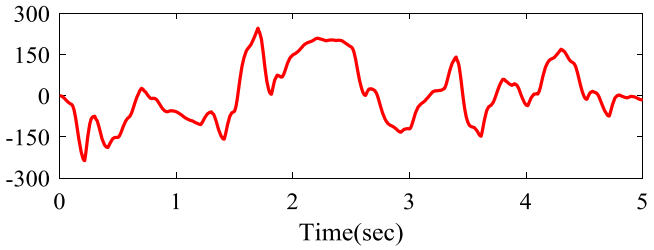

Fig. 4. The variation of the control input force $u(t)$/(N).

The responses of sprung-mass acceleration, suspension dynamic displacement and tire dynamic load for this active suspension with the CABT, SMC and PS system are shown in Fig. 3. It is obvious from Fig. 3(a) that the sprung-mass acceleration with the proposed CABT controller has been greatly reduced compared to the SMC and PS system. Specifically, it is seen from Fig. 3(b) to (c) that the suspension dynamic displacement is less than the maximum limit value $\Delta y_{\max}$=0.05 m, and the fluctuation of tire dynamic load is smooth and stable with the decreasing amplitude. Compared with the SMC, our proposed CABT controller can better realize the coordinated control over the sprung mass acceleration and suspension dynamic displacement, simultaneously, and those two performance indicators have also an improvement. The variation of $u(t)$ generated by the proposed CABT controller is given in Fig. 4. It is found out that $u(t)$ is all less than its maximal value of $u_{\max}$.

Fig. 5 shows the tracking trajectories of $x_1(t)$ and $x_2(t)$ under C-class road disturbance. It is apparent that both $x_1(t)$ and $x_2(t)$ are in accord with $x_{1r}(t)$ and $x_2^d(t)$ in the MRS.

To analyze the variation of these three performance indicators with the change of M_s, the simulation is performed and the results are shown in Figs. 6–8. It can be observed that the changes of M_s have little impacts on vehicle dynamics performances for the CABT controller. Yet, it may cause the inconsistency of vehicle dynamic performances for the PS system.

To further evaluate the proposed CABT controller under different operating conditions, four different vehicle speeds of 20 m/s, 25 m/s, 30 m/s and 35 m/s are chosen to conduct the simulation analysis on the CABT and PS system under the different types of road disturbance inputs like A Grade (Good), B Grade (Average), C Grade (Poor), and D Grade (Very Poor) road surfaces.

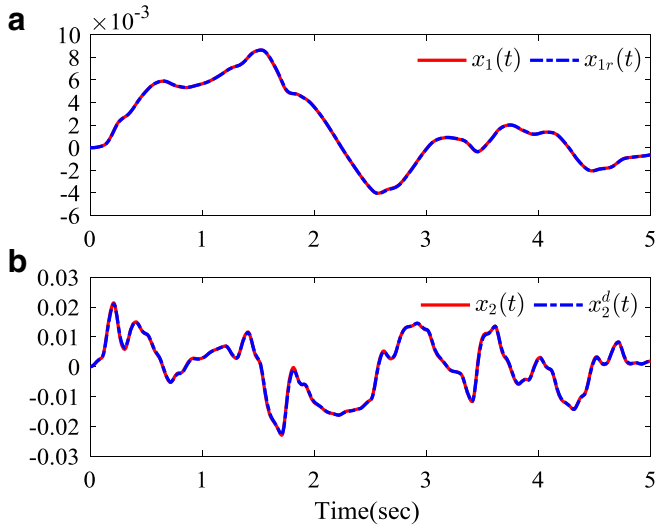

Fig. 5. The tracking trajectories of (a) $x_1(t)$ and (b) $x_2(t)$ under C-class road disturbance.

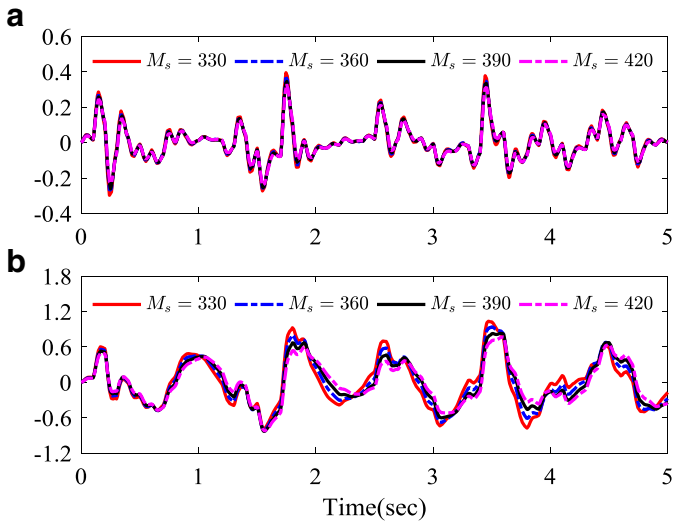

Fig. 6. The responses of sprung-mass acceleration (m/s^2) for (a) CABT and (b) PS system with various sprung masses.

The root-mean-square (RMS) values of the vehicle dynamics performance indicators are calculated, simultaneously, and the related RMS values are presented in Fig. 9. It can be seen that, in comparison with the PS system, the CABT controller can always maintain a lower RMS value with a smooth change, which further illustrates that the proposed CABT controller has good robustness and adaptability to the parameters uncertainties, the variations of vehicle speeds as well as the road disturbances.

4.2. Performance of the CABT controller under bump road

A pronounced bump on a smooth road surface is usually adopted to validate the performance of the designed controller, which is given by [15]

$$\dot{z}_r(t) = \frac{\pi V A_m}{L} \sin \frac{2\pi V}{L} t, \qquad 0 \le t \le \frac{L}{V} \tag{46}$$

where A_m and L are the height and length of the bump road disturbance, respectively. It is assumed that $A_m = 0.1$ m and $L = 5$ m, and $V = 10$ m/s. Here the simulation results are shown in Fig. 10.

We can observe that the performance responses of the proposed CABT controller and the common SMC are obviously improved with converging to zero within a finite time, in comparison with those of the PS system. Furthermore, it can be

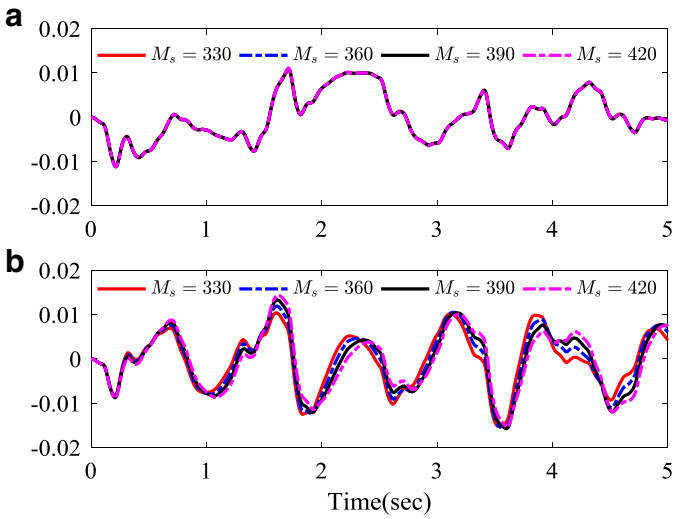

Fig. 7. The responses of suspension dynamic displacement (m) for (a) CABT and (b) PS system with various sprung masses.

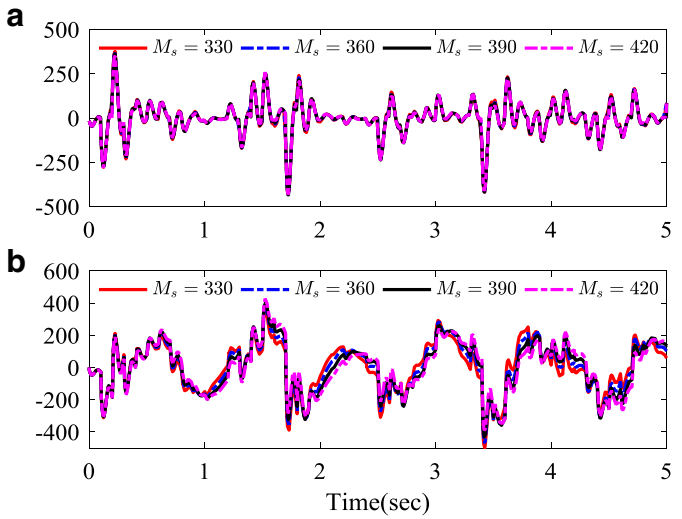

Fig. 8. The responses of tire dynamic load (N) for (a) CABT and (b) PS system with various sprung masses.

Table 2
RMS comparisons of three performance indicators under bump road disturbance.

Performed	CABT	SMC	PS
Sprung-mass acceleration	0.7632 (↓ 62.6%)	0.7837 (↓ 61.5%)	2.0407 (–)
Suspension dynamic displacement	0.0206 (↓ 33.8%)	0.0237 (↓ 23.8%)	0.0311 (-)
Tire dynamic load	388 (↓ 45.7%)	404 (↓ 43.4%)	715 (–)

concluded that the proposed CABT controller has better dynamic performances and a shorter convergence time with respect to the SMC system.

Additionally, Fig. 11 shows the tracking trajectories of $x_1(t)$ and $x_2(t)$ under bump road disturbance. It is apparent that the variations of $x_1(t)$ and $x_2(t)$ are in accord with their corresponding reference trajectories, which illustrates that the proposed CABT controller has better tracking performances.

Finally, Table 2 summarizes the RMS comparisons of the three performance indicators for the active suspension system with the CABT, SMC and PC system under bump road disturbance. It is seen from Table 2, compared to the PS system, the RMS values of the aforementioned three performance indicators with the CABT and SMC controller are reduced about 62.6%,

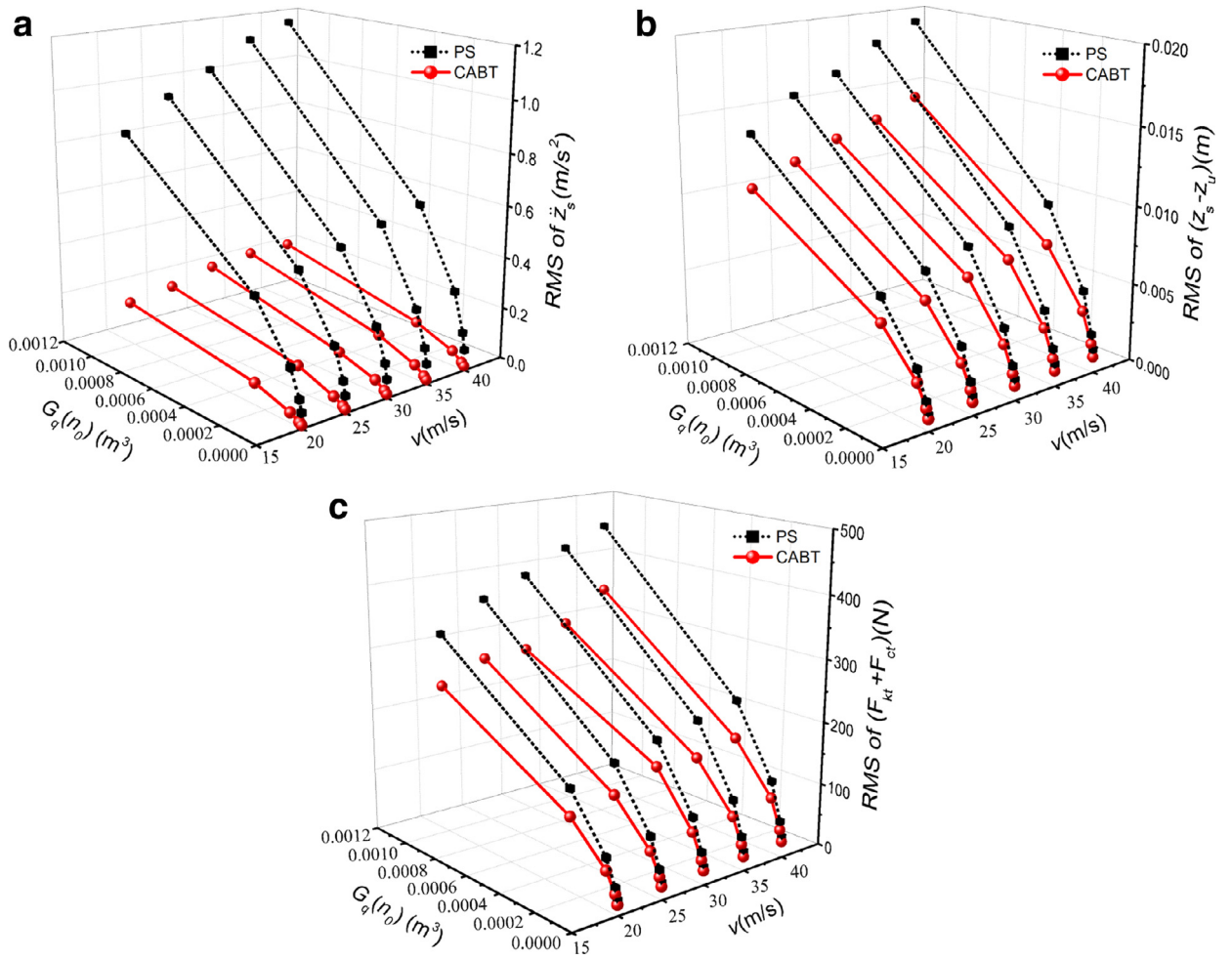

Fig. 9. The responses of (a) sprung-mass acceleration, (b) suspension dynamic displacement, and (c) tire dynamic load for the CABT and PS system with various vehicle speeds and road surfaces.

33.8%, 45.7%, and 61.5%, 23.8%, 43.4%, respectively, under the bump road disturbance. This shows that the proposed CABT controller can improve vehicle ride quality while satisfying the safety performance constraints under bump road profiles, which further illustrates that the designed controller has better control performances.

4.3. Comparative simulation investigations

The comparative simulations are performed to evaluate the proposed CABT controller for the same quarter-vehicle model, which is based on the operating scenario including the same reference trajectories and initial values, as well as the same road surface disturbance. The plots of this CABT controller are provided and compared with the corresponding ones of the ABC in [16,27], wherein the simulation results in Figs. 12–17 are categorized into two simulation cases as Case 1 and Case 2, and the detailed descriptions are summed up as:

(1) The performance indicators of ride comfort as the sprung-mass acceleration and displacement, and the safety performance indicators as tire dynamic load, suspension dynamic displacement and active control force are compared, respectively.
(2) The validation of tracking errors of the sprung-mass displacement and vertical velocity is conducted, simultaneously.

- **Case 1: performance analysis under random road**

Fig. 12 displays the comparisons of sprung-mass displacement, sprung-mass acceleration, suspension dynamic displacement and tire dynamic load for the same quarter-active suspension with the ABC in [16,27] and the proposed CABT controller. It can be confirmed from Fig. 12(a) to (b) that compared to the ABC in [16], our previous study in [27], the sprung-mass acceleration and displacement with the CABT controller can be reduced with smaller amplitude. Moreover, according to Fig. 12(c) to (d), it is seen that both the ABC in [16,27] can also achieve the safety performance constraints as suspension

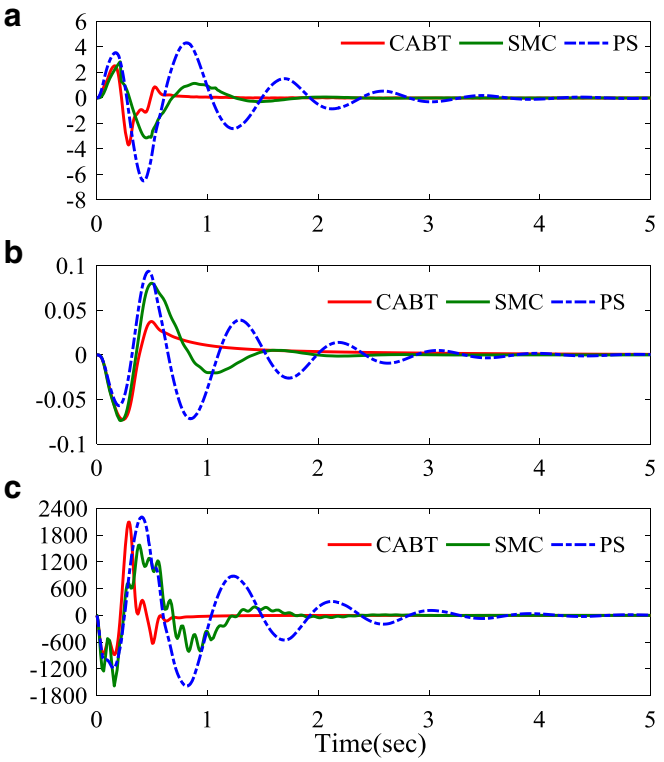

Fig. 10. The responses of (a) sprung-mass acceleration (m/s^2), (b) suspension dynamic displacement (m) and (c) tire dynamic load (N) for the CABT, SMC and PS system under bump road disturbance.

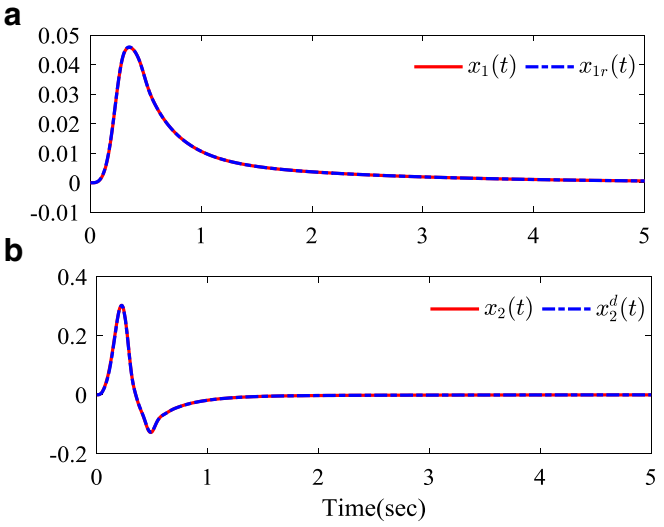

Fig. 11. The tracking trajectories of (a) $x_1(t)$ and (b) $x_2(t)$ under bump road disturbance.

dynamic displacement and tire dynamic load, yet the proposed CABT controller has better control effects in suspension dynamic displacement and tire dynamic load. Fig. 13 shows the variations of $u(t)$ with these three controllers under C-class random road disturbance, it is apparent that the amplitude of the three types of ABCs are retained within the range of -300 to 300 N. Fig. 14 shows the tracking errors of $e_1(t)$ and $e_2(t)$ for this active suspension system with the three controllers under the same road disturbance. By analyzing Fig. 14, it is easily seen that the tracking errors of $e_1(t)$ and $e_2(t)$ for the proposed CABT controller has smoother trend with the smaller amplitude as compared to the ABC in [16,27], which demonstrates that the proposed CABT controller has better control effects.

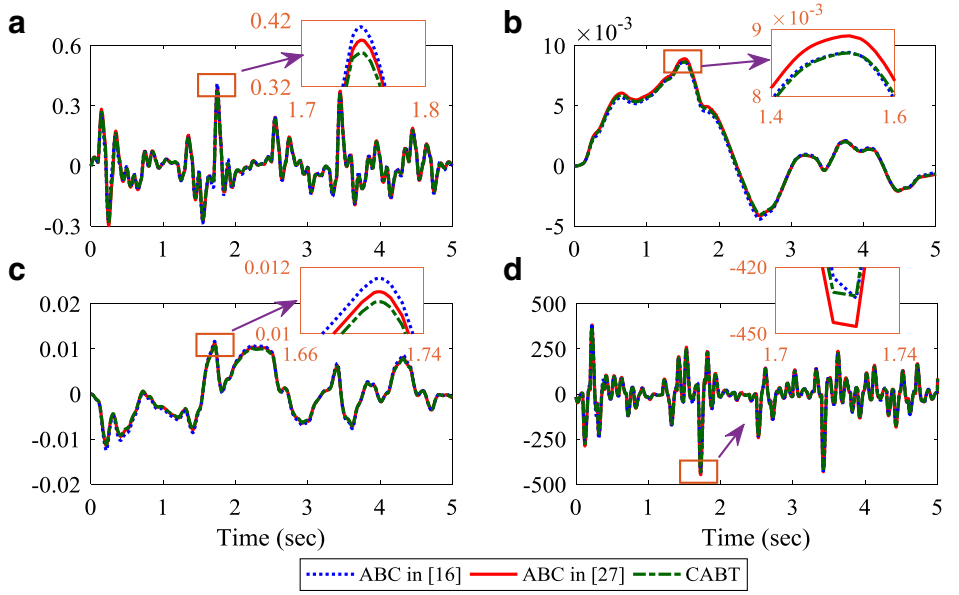

Fig. 12. The comparisons of (a) sprung-mass acceleration (m/s^2), (b) sprung-mass displacement (m), (c) suspension dynamic displacement (m), and (d) tire dynamic load (N) for the ABC in [16,27], and the proposed CABT controller under C-class road disturbance.

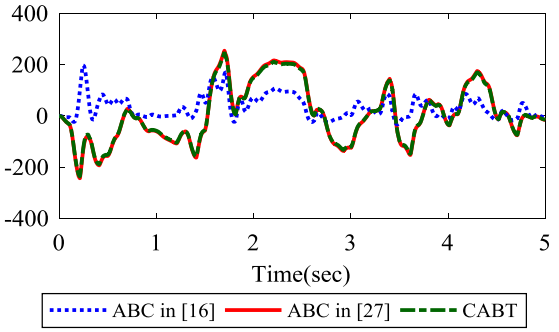

Fig. 13. The variations of $u(t)$/(N) for the three controllers under C-class road disturbance.

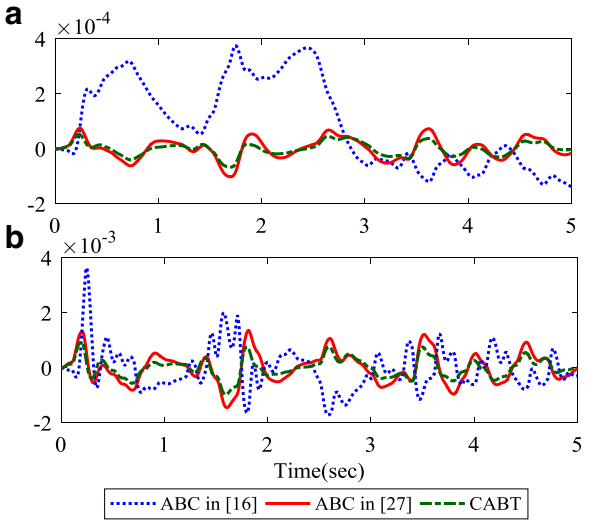

Fig. 14. The tracking errors of (a) $e_1(t)$ (m) and (b) $e_2(t)$ (m/s) for the three controllers under C-class road disturbance.

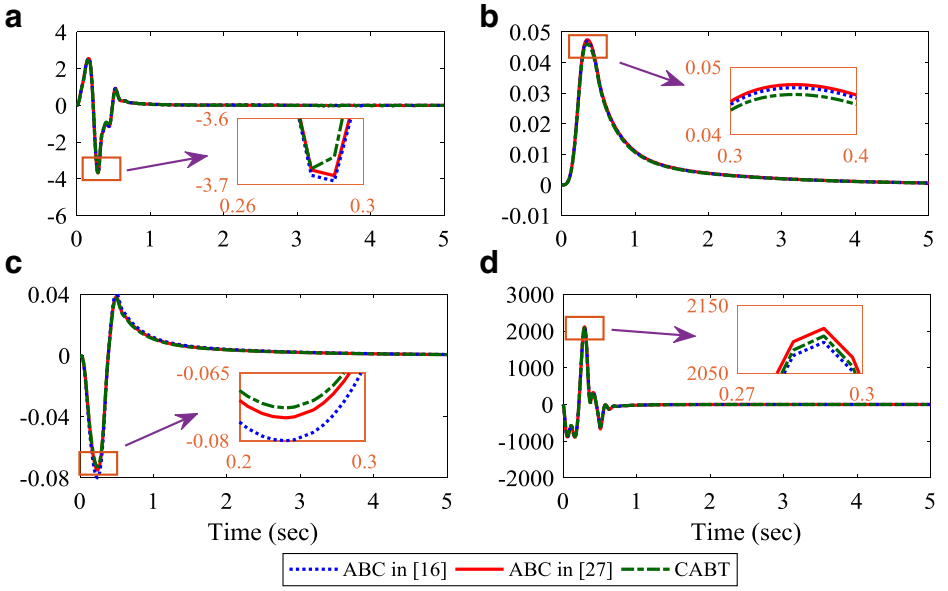

Fig. 15. The comparisons of (a) sprung-mass acceleration (m/s^2), (b) sprung-mass displacement (m), (c) suspension dynamic displacement (m) and (d) tire dynamic load (N) for the ABC in [16,27] and the proposed CABT controller under bump road disturbance.

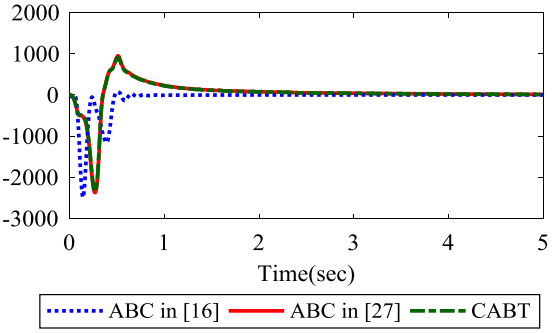

Fig. 16. The variation of $u(t)$/(N) for the three controllers under bump road disturbance.

- **Case 2: performance analysis under bump road**

Similarly, Fig. 15 displays the comparisons of sprung-mass acceleration, sprung-mass displacement, suspension dynamic displacement and tire dynamic load for the same control plant with the ABC in [16,27] and the proposed CABT controller. Also, it is easily seen from Fig. 15(a) to (b) that, in contrast with the performance indicators using the ABC in [16,27], the sprung-mass acceleration and displacement can be decreased a little bit, and both of them can reach into a relative stability state within a shorter time. As shown in Fig. 15(c), the suspension dynamic displacement with the proposed CABT controller has a relatively smaller positive peak value. Additionally, from Fig. 15(d), the tire dynamic load with the three types of ABC can definitely ensure the firm uninterrupted contact of wheels to road. Moreover, it can be inferred from Fig. 16 that the control input forces $u(t)$ has the same trend with a maximal control force less than $u_{\max}$=3000 N, which satisfies the actuator input saturation requirement.

Fig. 17 reveals the tracking errors of $e_1(t)$ and $e_2(t)$ for active suspension system with these three ABCs under bump road disturbance. It is observed from Fig. 17 that the tracking errors of $e_1(t)$ and $e_2(t)$ for the proposed CABT controller can converge to zero within less time, respectively, which demonstrates the proposed controller has better control performances than those of the ABC in [16,27].

To sum up, one can get the following remarks as:

- On the whole, the amplitudes of this active suspension performances show a similar trend under bump road disturbance, yet the active suspension with the proposed CABT controller has the smallest peak values of sprung-mass acceleration, sprung-mass displacement and dynamic suspension displacement as compared with the ABC in [16,27], respectively;
- The tracking errors of $e_1(t)$ and $e_2(t)$ for the CABT controller are less than those of the ABC in [16,27], in particular they can be asymptotically convergent to a stable state within a shorter time.

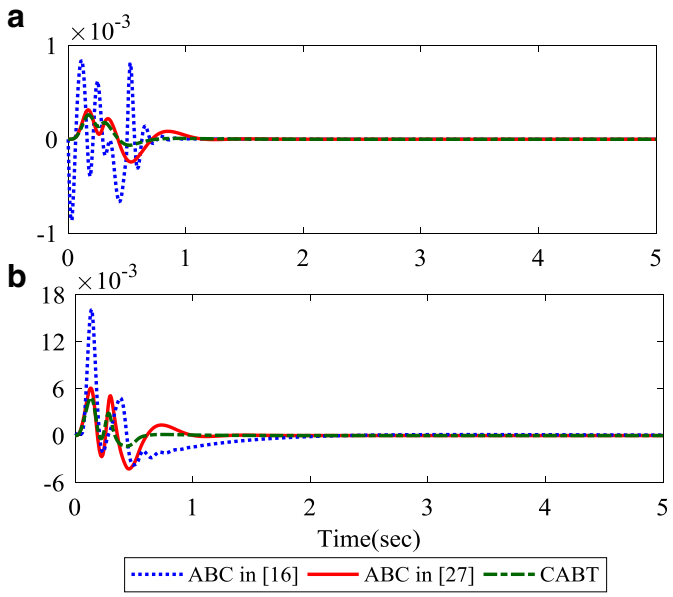

Fig. 17. Tracking error of (a) $e_1(t)$ (m) and (b) $e_2(t)$ (m/s) for the three controllers under bump road disturbance.

5. Conclusions

In this paper, a novel adaptive backstepping tracking control for nonlinear active suspension system considering parameter uncertainties was proposed to achieve the coordinated control over the sprung-mass acceleration and suspension dynamic displacement. An MRS was first established to provide the ideal reference trajectories of the sprung-mass displacement and vertical velocity. Second, an adaptive backstepping control law was synthetically developed, and the tracking errors of the sprung-mass displacement and vertical velocity between the CABT and the MRS were defined to make the control plant accurately track the prescribed performances of the MRS, which could stabilize the vertical motion of vehicle body. Finally, a numerical example was provided to demonstrate the effectiveness of the proposed control approach under different scenarios.

(1) By analyzing Sections 4.1 and 4.2, one can get that each performance indicator of this active suspension with the proposed CABT controller has the small fluctuations and can be convergent to zero in a shorter time, which illustrates that the closed-loop system is more stable and has better control effects in comparison with the SMC and PS system.
(2) From the discussions of Case 1 and Case 2 in Section 4.3, it is obvious that, compared with the ABC in [16,27], each performance curve with the CABT controller has smaller peak values and the tracking errors of $e_1(t)$ and $e_2(t)$ for the CABT controller are more closer to zero, which shows that the designed CABT controller has highest accuracy among these three ABC approaches.
(3) For the ABC design in literature [16,27], a linear feedback term $e_i(t)$ is used and it may lead to higher conservatism, wherein the controller parameters are restrained within a smaller range. Therefore, we employ a constrained hyperbolic tangent function $\tanh(e_i(t))$ to replace the linear feedback term $e_i(t)$ in the ABC in [16] and ABC in [27], with aiming to improve the robustness of the proposed CABT controller.

Additionally, we must admit that the limitations of this CABT controller is that the control effect of tire dynamic load is not better as expected, thus our future work will focus on designing the multi-objective coordinated optimization control of sprung-mass acceleration, suspension dynamic displacement and tire dynamic load on active suspension system, and further developing the testbed to verify the effectiveness of the designed CABT controller.

Acknowledgments

The author would like to thank the Editor in Chief Professor Johann Sienz, and the innominate Associate Editor and reviewers for their constructive comments during the course of article revision. This work is supported by the National Natural Science Foundation of China under Grant 51675423 and 51305342, and Primary Research & Development Plan of Shaanxi Province under Grant 2017GY-029, which is gratefully acknowledged by the authors.

Conflict of interest

The authors of this paper declare that they have no conflict of interest.

References

[1] M. Canale, M. Milanese, C. Novara, Semi-Active suspension control using “fast” model-predictive techniques, IEEE Trans. Control Syst. Technol. 14 (2006) 1034–1046.
[2] S.M. Savaresi, C. Spelta, A single-sensor control strategy for semi-active suspensions, IEEE Trans. Control Syst. Technol. 17 (2009) 143–152.
[3] A.F Naudé, J.A. Snyman, Optimisation of road vehicle passive suspension systems. Part 2. Qualification and case study, Appl. Math. Modell. 27 (2003) 263–274.
[4] H. Gao, J. Lam, C. Wang, Multi-objective control of vehicle active suspension systems via load-dependent controllers, J. Sound Vib. 290 (2006) 654–675.
[5] J. Cao, P. Li, H. Liu, An interval fuzzy controller for vehicle active suspension systems, IEEE Trans. Intell. Transp. Syst. 11 (2010) 885–895.
[6] W. Sun, Y. Zhao, J. Li, L. Zhang, Active suspension control with frequency band constraints and actuator input delay, IEEE Trans. Indust. Electron. 59 (2012) 530–537.
[7] Z. Zengnian, L. Feng, W. Yongbin, L. Changgang, Study on active suspension control of full-vehicle steering model of using DSP, in: Proceedings of the IEEE Vehicle Power & Propulsion Conference, IEEE, 2008.
[8] C.P. Cheng, C.H. Chao, T.H.S. Li, Design of observer-based fuzzy sliding-mode control for an active suspension system with full-car model, in: Proceedings of the IEEE International Conference on Systems, 25, 2010, pp. 1939–1944.
[9] J.W. Hu and J.S. Lin, Nonlinear control of full-vehicle active suspensions with backstepping design scheme, IFAC Proceedings Volumes 41(2008) 3404–3409.
[10] C.J. Huang, J.S. Lin, C.C. Chen, Road-adaptive algorithm design of half-car active suspension system, Expert Syst. Appl. 37 (2010) 4392–4402.
[11] J.H. Zhang, P Guo, J.W. Lin, K.N. Wang, A mathematical model for coupled vibration system of road vehicle and coupling effect analysis, Appl. Math. Modell. (2005).
[12] H. Du, N. Zhang, Fuzzy control for nonlinear uncertain electrohydraulic active suspensions with input constraint, IEEE Trans. Fuzzy Syst. 17 (2009) 343–356.
[13] W. Sun, H. Pan, Y. Zhang, H. Gao, Multi-objective control for uncertain nonlinear active suspension systems, Mechatronics 24 (2014) 318–327.
[14] H. Du, N. Zhang, J. Lam, Parameter-dependent input-delayed control of uncertain vehicle suspensions, J. Sound Vib. 317 (2008) 537–556.
[15] H. Li, J. Yu, C. Hilton, H. Liu, Adaptive sliding-mode control for nonlinear active suspension vehicle systems using T-S fuzzy approach, IEEE Trans. Indust. Electron. 60 (2013) 3328–3338.
[16] N. Yagiz, Y. Hacioglu, Backstepping control of a vehicle with active suspensions, Control Eng. Pract. 16 (2008) 1457–1467.
[17] J. Zhou, C. Wen, G. Yang, Adaptive backstepping stabilization of nonlinear uncertain systems with quantized input signal, IEEE Trans. Autom. Control 59 (2014) 460–464.
[18] T. Wang, Y. Zhang, J. Qiu, H. Gao, Adaptive fuzzy backstepping control for a class of nonlinear systems with sampled and delayed measurements, IEEE Trans. Fuzzy Syst. 23 (2015) 302–312.
[19] F.J. Lin, L.T. Teng, P.H. Shieh, Intelligent adaptive backstepping control system for magnetic levitation apparatus, IEEE Trans. Magn. 43 (2007) 2009–2018.
[20] R. Kalaivani, P. Lakshmi, Adaptive backstepping controller for a vehicle active suspension system, in: Fourth International Conference on Sustainable Energy & Intelligent Systems, IET, 2015.
[21] Y. Yang, S.C. Tan, S.Y.R. Hui, Adaptive reference model predictive control with improved performance for voltage-source inverters, IEEE Trans. Control Syst. Technol. PP (99) (2018) 1–8.
[22] K.E. Majdoub, F. Giri, F.Z. Chaoui, Backstepping adaptive control of quarter-vehicle semi-active suspension with dahl MR damper model, in: Proceedings of the IFAC Proceedings Volumes, 46, 2013, pp. 558–563.
[23] Y. Savas, H.I. Basturk, Adaptive backstepping control design for active suspension systems actuated by four-way valve-piston, in: Proceedings of the American Control Conference, IEEE, 2017.
[24] X. Su, Master–Slave control for active suspension systems with hydraulic actuator dynamics, IEEE Access 5 (2017) 3612–3621.
[25] H. Li, X. Jing, H.R. Karimi, Output-feedback-based H_∞ control for vehicle suspension systems with control delay, IEEE Trans. Ind. Electron. 61 (2014) 436–446.
[26] W. Sun, H. Gao, O. Kaynak, Adaptive backstepping control for active suspension systems with hard constraints, IEEE/ASME Trans. Mechatron. 18 (2013) 1072–1079.
[27] H. Pang, X. Zhang, Z. Xu, Adaptive backstepping-based tracking control design for nonlinear active suspension system with parameter uncertainties and safety constraints, ISA Trans. 88 (2019) 23–36.
[28] J.S. Lin, I. Kanellakopoulos, Nonlinear design of active suspensions, in: Proceedings of the IEEE Conference on, IEEE, 1997.
[29] M. Sun, A barbalat-like lemma with its application to learning control, IEEE Trans. Autom. Control 54 (2009) 2222–2225.
[30] International Organization for Standardization, online: https://www.iso.org/committee/51514/x/catalogue/.